2013 IEEE/RSJ International Conference on
Intelligent Robots and Systems (IROS)
November 3-7, 2013. Tokyo, Japan

Model of cyclotorsion in a Tendon Driven Eyeball: theoretical model and qualitative evaluation on a robotic platform

Francesco Nori[1], Giulio Sandini[1], Giorgio Metta[1]

Abstract— **In this paper we describe the mathematical model of a tendon driven eye. We focus on describing its movements, posing a specific attention on cyclotorsion, that is the rotation around the eye optical axis. This study aims at understanding the cause of a cyclotorsion effect that has been noticed on a real setup. The paper starts from a qualitative analysis of the effect. Then, it proposes two different models for its motion. Finally both models are validated by comparing their predictions with the outcomes on the real robot. Given the complexity of the system and of its motion results are for the moment just qualitative and quantitative comparison will be the goal of our future works.**

I. Introduction

In this paper we describe the tendon driven eye whose picture is given in Figure 1. The tendons are actuated by two motors, one for the vertical tendon and one for the horizontal tendon. The tension on the tendon is maintained by a spring which pushes on the cable. Figure 1 shows also a scheme of the horizontal section. The vertical section is similar.

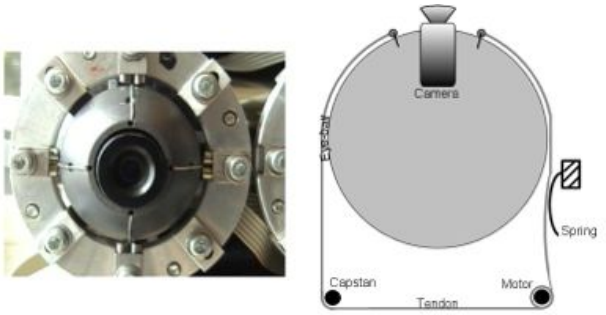

Fig. 1. The left picture shows the tendon driven eye. The two tendons are actuated by two motors. The first motor moves the vertical tendon. The second motor moves the horizontal tendon. The right figure sketches the actuation scheme.

II. Cyclotorsion

The present paper focuses on a cyclotorsion effect that was noticed on the real setup. With the term cyclotorsion we indicate a rotation around the optical axis of the camera (see Figure 1).

This work was supported by the following EC projects: CoDyCo, (FP7-ICT-2011.2.1 number 600716) and Xperience (FP7-ICT-2009.2.1 number 270273) .

[1]Francesco Nori and Giulio Sandini are with Robotics, Brain and Cognitive Sciences at the Istituto Italiano di Tecnologia. Giorgio Metta is with the iCub Facility at the Istituto Italiano di Tecnologia. name.surname(at)iit.it

Fig. 2. In order to measure the eye cyclotorsion, a calibration panel was placed in front of the camera. The figure shows a typical picture taken by the camera.

Let us briefly describe the undesired effect. In the current implementation the two motors are commanded in position. It was noticed that the same position of the motors does not correspond a unique configuration of the eyeball. In particular, starting in a particular configuration of the eyeball and following a cyclic path[1] with the motors, the systems does not return to the initial configuration and presents an evident rotation around the optical axis. The cause of the experienced phenomena is clearly the lack of a direct control on the system cyclotorsion.

Clearly, this phenomena is undesired since it doesn't allow to reconstruct the position of the eyeball given the position of the motors. In order to give a first characterization of the problem, we designed an experimental setup based on the use of the Hough transform [4]. The idea consists in placing, in front of the camera, a panel where a vertical line is painted (see Figure 2). In order to measure the cyclotorsion angle, we used the images taken from the camera which is mounted on the eyeball. In its initial configuration, the camera points towards a panel. Let α_0 be the slope of the painted line. Motors are then moved on cyclic path (i.e. the motor positions is exactly the same after each path execution). After each cycle, the cyclotorsion of the eyeball changes and consequently the slope α of the line changes (see Figure 3). The amount of cyclotorsion β corresponds to the difference in the line orientation, i.e. $\beta = \alpha - \alpha_0$. The slope of the line in the image has been computed using the Hough transform which is practically, a probability density of lines in the image plane.

A. Previous works

Many eye-head systems have been designed and built in the last year but very few mimics the human musculoskeletal

[1]Practically, a cyclic path of the motors correspond to a series of movements that start and finish in a unique configuration.

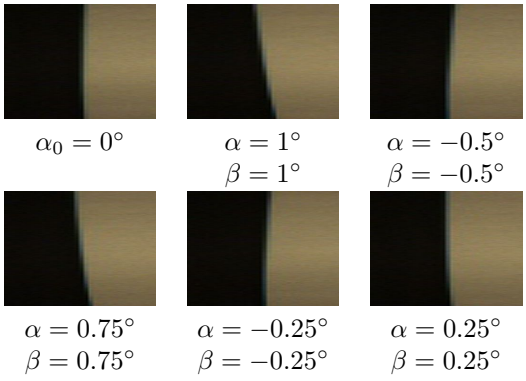

Fig. 3. This picture shows the line that has been used to measure the cyclotorsion; α is the slope of the line in the image and $\beta = \alpha - \alpha_0$ is the corresponding cyclotorsion. In order to see the changes of orientation (which are very small and less than $2°$), the pictures have been zoomed ten times horizontally. The rightmost picture was taken at the beginning of the experiment. The following pictures, from left to right, have been obtained after some cyclic paths of the motors (i.e. motors are in the same position in all the pictures shown here).

apparatus like the one described and analyzed in the present paper. Typically, the goal has been the one of achieving two principal movements (typically named a pan and a tilt movement) but very few systems were free to move along the cyclotorsion axis. On the contrary a lot of work has been done on the analysis, modeling and control of human-like eye movements [7], [6], [8]

Some recent works have proposed mechanical design with strong similarities with humans. Among this designs it is worth citing the work conducted by Cannata et al., [1], [3] on the development of a complex tendon driven robotic eye whose motion dynamics and relations with the Listing's Law have been analyzed in deep. The system consists of a sphere, actuated by four independent tendons driven by four motors with the eye-ball hold by a low friction support which allows three rotational degrees of freedom.

III. Motivating the analysis of cyclotorsion

As scientists, we are not only interested in measuring the cyclotorsion of the eyeball but also in understanding its causes. Clearly, in our specific case, the causes of cyclotorsion are not so evident. Apparently, the two tendons do not provoke any cyclotorsion on the system. Therefore the question is: what does provoke the observed cyclotorsion? Answering this question will give us insight in the kinematics of the systems suggesting elegant solutions to the encountered problem.

In the rest of the paper we will try to demonstrate that the observed cyclotorsion is a consequence of the system kinematics. The paper is divided into four sections. Section IV describes a mathematical model of the path described by the tendons. Section V describes two different kinematic models of the tendon driven eyeball; the first model is unrealistic and is introduced only to simplify the presentation of the following, more realistic model. Section VI shows the numerical results obtained by integrating the two kinematic models; it is observed that the given models present a cyclotorsion effect similar to that observed in the real setup. Finally, Section VII gives a qualitative comparison between results obtained in simulation and with the real setup.

IV. Mathematical model of the tendon geometry

Since the tendons are responsible for the movements of the eyeball, it is fundamental to describe the configuration assumed by given the configuration of the eyeball. In particular, in the present section we give the tools for computing the position of the tendons given the position of the eyeball.

We used MATLAB to create a model of the eye. The assumption is that the tendons are attached to the eyeball in the points E_1, E_2, E_3, and E_4. At the same time the tendons are forced to pass through the points C_1, C_2, C_3 and C_4 whose position is fixed with respect to an inertial reference frame (see Figure 4). Consider an inertial reference frame Σ_i, and let Σ_e be a reference frame attached to the eyeball. The origin of the two reference frames are assumed to overlap. Practically, the points E_1, E_2, E_3, E_4 are fixed in Σ_e and C_1, C_2, C_3, C_4 are fixed in Σ_i. We will use the following notation: E_j^i are the coordinates of E_j in Σ_i; E_j^e are the coordinates of E_j in Σ_e.

Let's now compute the position of the tendon passing through C_j to E_j. The assumption is that the tendon lies on the geodesic path connecting C_j to E_j. The geodesic path on the eyeball can be easily computed since its surface is spherical. Let C_j^i to E_j^i be the coordinated of C_j to E_j in the inertial reference frame Σ_i. The generic point G on the geodesic satisfies the following[2]:

$$\begin{cases} (C_j^i \times E_j^i) \cdot G^i = 0 \\ \left\| G^i \right\|^2 = r^2 \end{cases} \tag{2}$$

where r is the eyeball radius, $\times$ is the cross product, $\cdot$ is the dot product and G^i are the coordinates of G in the reference frame Σ_i. The length of the geodesic connecting C_j^i to E_j^i is given by:

$$\cos^{-1}\left(\frac{C_j^i \cdot E_j^i}{r^2}\right) r. \tag{3}$$

V. Kinematic model of the tendon driven eye

We here describe a kinematic model of the tendon driven eye. The section is divided into two subsections. We first consider a simplified model where a single tendon is used to push and to pull. Then we consider a more realistic model where tendons are only allowed to pull.

[2]The above conditions guarantees that G lies on the great circle that passes through C_j and E_j. To guarantee that the G is on the geodesic, we need also to impose the following conditions:

$$\begin{cases} C_j^i \cdot G^i \geq C_j^i \cdot E_j^i \\ E_j^i \cdot G^i \geq C_j^i \cdot E_j^i \end{cases} \tag{1}$$

which guarantee that the (geodesic) distance between G and E_j and the distance between G and C_j do not exceed the distance between C_j and E_j.

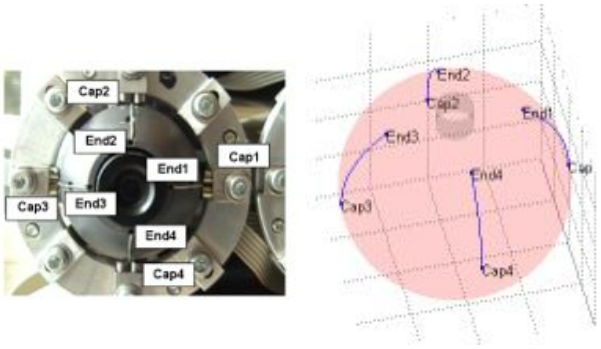

Fig. 4. The picture (left) and the sketch (right) show the points E_1, E_2, E_3, and E_4 which are attached to the eyeball. The points C_1, C_2, C_3 and C_4 are instead in fixed with respect to an inertial reference frame.

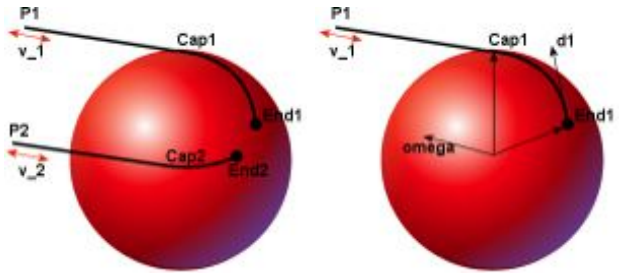

Fig. 5. The left picture shows the two tendons considered in the simplified kinematic model. Each tendon pushes and pulls the corresponding E_j. The right picture shows the situation $v_2 = 0$. Notice that in this situation the angular velocity ω^s is orthogonal to the plane generated by E_1 and C_1. Moreover, the norm of the vector ω^s can be determined imposing the constant length of the cable, i.e $v_{E_1} \cdot d_1 = v_1$.

A. Push-pull tendons

In the real setup one tendon connects E_1, C_1, C_3 and E_3. The other tendon connects E_2, C_2, C_4 and E_4. When the first motor rotates in one direction, the tendon pulls E_1. When it rotates in the opposite direction, the tendon pulls E_3. We here consider a simplified model, assuming that the motor pushes and pulls E_1 (see left Figure 5). The other side of the tendon (the one connected to E_3) is negligible in this framework and will be therefore omitted; the tendon terminates with the point P_1 whose velocity will be denoted v_1 (see right Figure 5). Similarly, we assume that the second motor pushes and pulls E_2. Again, the tendon terminates in the point P_2 whose velocity will be denoted v_2.

How does v_1 and v_2 constrain the instantaneous spatial angular velocity ω^s (see [5] for a definition) of the eyeball? Let's first consider a simplified situation imposing a null velocity of the second tendon, i.e. $v_2 = 0$. In this simplified situation it can be easily seen that the angular velocity ω^s is orthogonal to the plane generated by C_1 and E_1 (see right Figure 5). Therefore:

$$\omega^s = \left(E_1^i \times C_1^i\right) k_1(v_1) \tag{4}$$

Fig. 6.

where $k_1 \in \mathbb{R}$ can be determined imposing a constant length of the tendon. Specifically, let d_1 be the tangent to the tendon in E_1 (see right Figure 5). Moreover, let v_{E_1} be the velocity of E_1, i.e.:

$$v_{E_1} = \omega^s \times E_1^i. \tag{5}$$

Then, in order to have a constant length of the tendon the projection of v_{E_1} along d_1 must be equal to v_1, i.e.:

$$v_{E_1} \cdot d_1 = v_1. \tag{6}$$

Substituting (5) into (6) we obtain:

$$\left(\omega^s \times E_1^i\right) \cdot d_1 = v_1, \tag{7}$$

which can be used to determine k_1. Similarly, if $v_1 = 0$ we have:

$$\omega^s = \left(E_2 \times C_2\right) k_2(v_2). \tag{8}$$

and again k_2 can be determined from:

$$\left(\omega^s \times E_2^i\right) \cdot d_2 = v_2. \tag{9}$$

Finally, in the more general case $v_1 \neq 0$ and $v_2 \neq 0$. In this case the velocity ω^s belongs to the plane generated by $E_1 \times C_1$ and $E_2 \times C_2$ since (5) and (8) both holds. We have:

$$\omega^s = \left(E_1^i \times C_1^i\right) k_1 + \left(E_2^i \times C_2^i\right) k_2. \tag{10}$$

Equivalently, we can write:

$$\omega^s \cdot \left[\left(E_1^i \times C_1^i\right) \times \left(E_2^i \times C_2^i\right)\right] = 0. \tag{11}$$

Once again we need to impose the two conditions on the length of the tendons. Specifically we have:

$$\left(\omega^s \times E_1^i\right) \cdot d_1 = v_1, \qquad \left(\omega^s \times E_2^i\right) \cdot d_2 = v_2, \tag{12}$$

which can be rewritten:

$$\omega^s \cdot \left(E_1^i \times d_1\right) = v_1, \qquad \omega^s \cdot \left(E_2^i \times d_2\right) = v_2. \tag{13}$$

Conditions (11) and (13) fully specify the angular velocity which turns out to be the unique solution of the following system in three unknowns and three constraints:

$$\begin{cases} \omega^s \cdot \left[\left(E_1^i \times C_1^i\right) \times \left(E_2^i \times C_2^i\right)\right] = 0 \\ \omega^s \cdot \left(E_1^i \times d_1\right) = v_1 \\ \omega^s \cdot \left(E_2^i \times d_2\right) = v_2. \end{cases} \tag{14}$$

where it can be proven that:

$$d_1 = \frac{\left(C_1^i \times E_1^i\right) \times E_1^i}{\left\|\left(C_1^i \times E_1^i\right) \times E_1^i\right\|}, \tag{15}$$

$$d_2 = \frac{\left(C_2^i \times E_2^i\right) \times E_2^i}{\left\|\left(C_2^i \times E_2^i\right) \times E_2^i\right\|}. \tag{16}$$

The above system can be rearranged with some trivial computations. In particular we have:

$$\begin{cases} \omega^s \cdot \left[\left(E_1^i \times C_1^i\right) \times \left(E_2^i \times C_2^i\right)\right] = 0 \\ \omega^s \cdot \left(E_1^i \times C_1^i\right) = \tilde{v}_1 \\ \omega^s \cdot \left(E_2^i \times C_2^i\right) = \tilde{v}_2. \end{cases} \tag{17}$$

with:

$$\tilde{v}_1 = \frac{\left\|\left(C_1^i \times E_1^i\right) \times E_1^i\right\|}{r^2} v_1, \tag{18}$$

$$\tilde{v}_2 = \frac{\left\|\left(C_2^i \times E_2^i\right) \times E_2^i\right\|}{r^2} v_2. \tag{19}$$

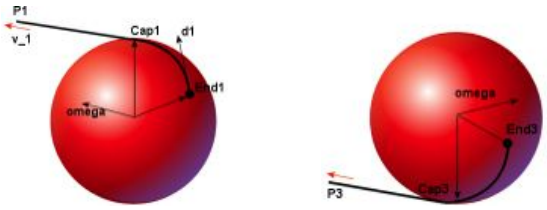

Fig. 7. A more realistic model takes into account the fact that tendons are only allowed to pull. The picture shows this situation. When the motor rotates in one direction, E_1 is pulled. When the motor rotates in the opposite direction E_3 is pulled.

B. Pull-only tendons

In a more realistic situation the tendons are only allowed to pull (see Figure 7). Therefore the above model needs to be changed. Let $v_1 > 0$ indicate the situation in which E_1 is pulled; similarly $v_2 > 0$ indicates that E_2 is pulled. Clearly, if $v_1 > 0$ and $v_2 > 0$ then Eq. (10) still holds. However, if $v_1 < 0$ and $v_2 > 0$ then E_3 and E_2 are pulled and the model must be changed. The left picture in Figure 7 shows that Eq. (10) must be modified as follows:

$$\omega^s = \left(E_3^i \times C_3^i\right) k_1 + \left(E_2^i \times C_2^i\right) k_2, \tag{20}$$

which corresponds to:

$$\omega^s \cdot \left[\left(E_3^i \times C_3^i\right) \times \left(E_2^i \times C_2^i\right)\right] = 0. \tag{21}$$

More generally, the model of the system is the following:

$$\begin{cases} \omega^s \cdot \left[\left(E_1^i \times C_1^i\right) \times \left(E_2^i \times C_2^i\right)\right] = 0 & \text{if } v_1 \geq 0, v_2 \geq 0 \\ \omega^s \cdot \left[\left(E_3^i \times C_3^i\right) \times \left(E_2^i \times C_2^i\right)\right] = 0 & \text{if } v_1 < 0, v_2 \geq 0 \\ \omega^s \cdot \left[\left(E_1^i \times C_1^i\right) \times \left(E_4^i \times C_4^i\right)\right] = 0 & \text{if } v_1 \geq 0, v_2 < 0 \\ \omega^s \cdot \left[\left(E_3^i \times C_3^i\right) \times \left(E_4^i \times C_4^i\right)\right] = 0 & \text{if } v_1 < 0, v_2 < 0 \\ \omega^s \cdot \left(E_1^i \times d_1\right) = v_1 \\ \omega^s \cdot \left(E_2^i \times d_2\right) = v_2. \end{cases} \tag{22}$$

This model is more complicated but more realistic. It can be used to uniquely determine ω^s given the velocities of the motors.

VI. Simulating the kinematic model

In this section we show the results obtained by integrating the kinematic models (14) and (22). The section is divided into two parts. The first subsection describes the procedure to write the kinematic models in the normal form. This step is fundamental if we want to integrate the models using standard softwares, such as MATLAB. The second subsection shows the numerical results obtained by integrating the two proposed kinematic models (14) and (22). It is observed that both models present a cyclotorsion effect similar to the one observed on the real setup.

A. Normal form of the kinematic model

The models (14) and (22) are practically differential equations that describe the kinematics of the two considered models. We here explicitly derive the normal form of the differential equation (14); the derivation of the normal form of (22) is very similar and therefore omitted. Let $R(t) \in SO(3)$ be the rotation matrix that maps points in the eye reference frame Σ_e into points the inertial reference frame Σ_i. Then the model (14) can be written as follows:

$$\begin{cases} \omega^s(t) \cdot \left[\left(R(t)E_1^e \times C_1^i\right) \times \left(R(t)E_2^e \times C_2^i\right)\right] = 0 \\ \omega^s(t) \cdot \left(R(t)E_1^e \times d_1(t)\right) = v_1(t) \\ \omega^s(t) \cdot \left(R(t)E_2^e \times d_2(t)\right) = v_2(t), \end{cases} \tag{23}$$

where:

$$E_j^i(t) = R(t)E_j^e, \quad d_j(t) = \frac{\left(C_j^i \times E_j^i(t)\right) \times E_j^i(t)}{\left\|\left(C_j^i \times E_j^i(t)\right) \times E_j^i(t)\right\|}. \tag{24}$$

The vector ω^s is related to the time derivative of $R(t)$ by the following relation (see [5]):

$$\hat{\omega}^s(t) = \dot{R}(t)R^\top(t). \tag{25}$$

Therefore, (23) can be rearranged as a differential equation in the *normal form*:

$$\dot{R} = f(R, v_1, v_2). \tag{26}$$

for a suitably defined function $f(\cdot)$. The differential equation above can be integrated from the initial condition $R(0) = R_0 \in SO(3)$ given the inputs $v_1(t)$ and $v_2(t)$. However, due to numerical errors we have that after few steps of integration $R(t)$ is no longer a rotation matrix, i.e. $R(t) \notin SO(3)$. To avoid these problems we can represent $R(t)$ in exponential coordinates $\psi(t) \in \mathbb{R}^3$ such that $R(t) = e^{\hat{\psi}(t)}$. We have [2]:

$$\dot{\psi} = \left(I + \frac{1}{2}\hat{\psi} + \left(1 - \alpha\left(\|\psi\|\right)\right) \frac{\hat{\psi}^2}{\|\psi\|^2}\right) \omega^b \tag{27}$$

where ω^b is the instantaneous body angular velocity [5], and $\alpha(y) = (y/2)\cot(y/2)$. The body angular velocity can be obtained modifying (14) as follows:

$$\begin{cases} \omega^b \cdot \left[\left(E_1^e \times e^{-\hat{\psi}} C_1^i\right) \times \left(E_2^e \times e^{-\hat{\psi}} C_2^i\right)\right] = 0 \\ \omega^b \cdot \left(E_1^e \times e^{-\hat{\psi}} d_1\right) = v_1 \\ \omega^b \cdot \left(E_2^e \times e^{-\hat{\psi}} d_2\right) = v_2, \end{cases} \tag{28}$$

Solving explicitly in the unknown ω^b:

$$\omega^b = \begin{bmatrix} E_1^e \times e^{-\hat{\psi}} d_1 \\ E_2^e \times e^{-\hat{\psi}} d_2 \\ \left(E_1^e \times e^{-\hat{\psi}} C_1^i\right) \times \left(E_2^e \times e^{-\hat{\psi}} C_2^i\right) \end{bmatrix}^{-\top} \begin{bmatrix} v_1 \\ v_2 \\ 0 \end{bmatrix}, \tag{29}$$

where $A^{-\top}$ indicates $\left(A^\top\right)^{-1}$. Substituting (29) into (27) we obtain the following normal form:

$$\dot{\psi} = \left(I + \frac{1}{2}\hat{\psi} + \left(1 - \alpha\left(\|\psi\|\right)\right) \frac{\hat{\psi}^2}{\|\psi\|^2} \right) \cdot \cdot \begin{bmatrix} E_1^e \times e^{-\hat{\psi}} d_1 \\ E_2^e \times e^{-\hat{\psi}} d_2 \\ \left(E_1^e \times e^{-\hat{\psi}} C_1^i\right) \times \left(E_2^e \times e^{-\hat{\psi}} C_2^i\right) \end{bmatrix}^{-\top} \begin{bmatrix} v_1 \\ v_2 \\ 0 \end{bmatrix}.$$

Alternatively, starting from (17) we can obtain a relatively simpler differential equation that describes the system kinematics:

$$\dot{\psi} = \left(I + \frac{1}{2}\hat{\psi} + \left(1 - \alpha\left(\|\psi\|\right)\right) \frac{\hat{\psi}^2}{\|\psi\|^2} \right) \cdot \cdot \begin{bmatrix} E_1^e \times e^{-\hat{\psi}} C_1^i \\ E_2^e \times e^{-\hat{\psi}} C_1^i \\ \left(E_1^e \times e^{-\hat{\psi}} C_1^i\right) \times \left(E_2^e \times e^{-\hat{\psi}} C_2^i\right) \end{bmatrix}^{-\top} \begin{bmatrix} \tilde{v}_1 \\ \tilde{v}_2 \\ 0 \end{bmatrix}.$$

Finally, a more realistic model can be derived from (22). This alternative model is here omitted since it can be trivially derived.

B. Integration of the kinematic model

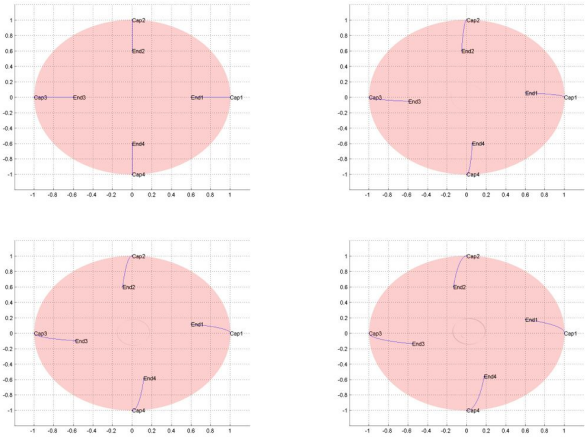

Fig. 8. Please zoom the .pdf for details. The figure shows four frontal snapshots of the eyeball. The rightmost picture corresponds to the initial condition $R(0) = I$. The other pictures, from right to left, corresponds to the configurations reached after one, two and three repetitions of closed path (30). The underlying kinematic model (14) assumes that the tendons push and pull.

We used MATLAB to integrate the normal forms of the kinematic models (14) and (22). The purpose of the simulation is to see if moving the eyeball generates a cyclotorsion movement, i.e. a rotation of the eyeball around the optical axis of the camera. In a first simulation, we have moved the tendons on the following closed path, i.e.:

$$v_1(t) = \begin{cases} \bar{v} & \text{if } t \in [0, \Delta] \\ 0 & \text{if } t \in [\Delta, 2\Delta] \\ -\bar{v} & \text{if } t \in [2\Delta, 3\Delta] \\ 0 & \text{if } t \in [3\Delta, 4\Delta] \end{cases}, \tag{30}$$

$$v_2(t) = \begin{cases} 0 & \text{if } t \in [0, \Delta] \\ \bar{v} & \text{if } t \in [\Delta, 2\Delta] \\ 0 & \text{if } t \in [2\Delta, 3\Delta] \\ -\bar{v} & \text{if } t \in [3\Delta, 4\Delta] \end{cases}. \tag{31}$$

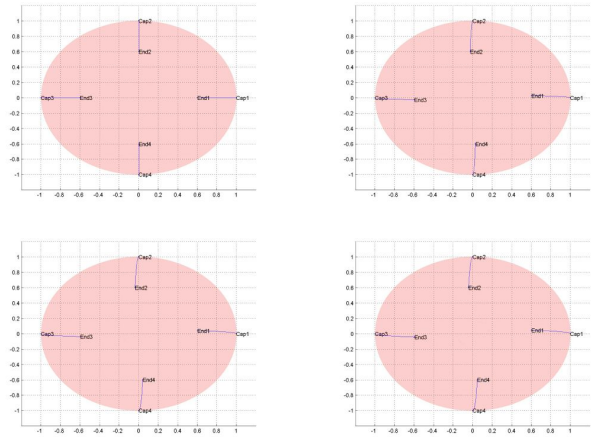

Fig. 9. Please zoom the .pdf for details. This picture is the analogous of Figure 8 but in this case the underlying kinematic model (22) assumes that the tendons only push.

where $\Delta > 0$ and $\bar{v}$ is a constant velocity. Repeating the same closed path a three times, we obtained the results shown in Figure 8 and Figure 9.

Figure 8 corresponds to the simplified model (14), which assumes that tendons can push and pull. Clearly, the systems present an evident cyclotorsion which increases after each closed path.

Figure 9 shows the results obtained with the more realistic model (22). In this case the cyclotorsion is still present but it is less evident and limited. Heuristically, simulations reveal that with this second model the cyclotorsion does not increase after each cycle: it initially increases but does not apparently increase after some cycles. This is not the case of the first model where cyclotorsion increases after each closed path.

In a second simulation we tested the possibility of producing a reverse cyclotorsion, in order to bring the eyeball back to the original configuration. In order to do this test we first moved the eyeball on the path (30) n times and then we moved the eyeball n times on the following inverse path:

$$v_1(t) = \begin{cases} 0 & \text{if } t \in [0, \Delta] \\ \bar{v} & \text{if } t \in [\Delta, 2\Delta] \\ 0 & \text{if } t \in [2\Delta, 3\Delta] \\ -\bar{v} & \text{if } t \in [3\Delta, 4\Delta] \end{cases}, \tag{32}$$

$$v_2(t) = \begin{cases} \bar{v} & \text{if } t \in [0, \Delta] \\ 0 & \text{if } t \in [\Delta, 2\Delta] \\ -\bar{v} & \text{if } t \in [2\Delta, 3\Delta] \\ 0 & \text{if } t \in [3\Delta, 4\Delta] \end{cases}. \tag{33}$$

Obtained results are illustrated in Figure 10 and Figure 11.

Figure 10 shows that the first model (14) is easily reversible since the inverse path drives the system back to the initial configuration.

Figure 11 shows that also in the second model (22) the inverse path produces an opposite cyclotorsion. However, the configuration reached by the system differs from the initial configuration.

VII. QUALITATIVE COMPARISON

In this section we report the results obtained in trying to replicate on the real system the experiments described

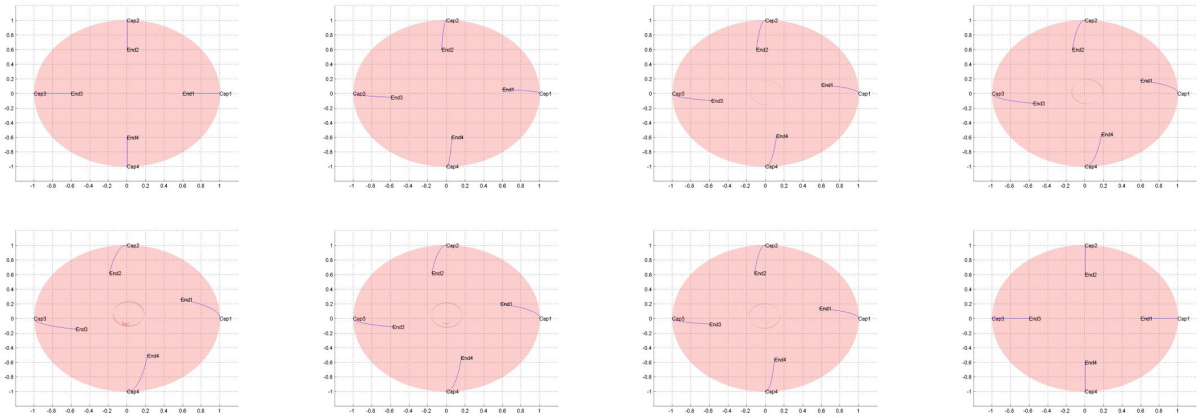

Fig. 10. Please zoom the .pdf for details. The figure shows eight frontal snapshots of the eyeball. The picture on the top right corner corresponds to the initial condition $R(0) = I$. The first row, from right to left, are the configurations reached after 3 repetitions of the direct path. The second row, is obtained by 3 repetitions of the inverse path. The underlying kinematic model (14) assumes that the tendons push and pull.

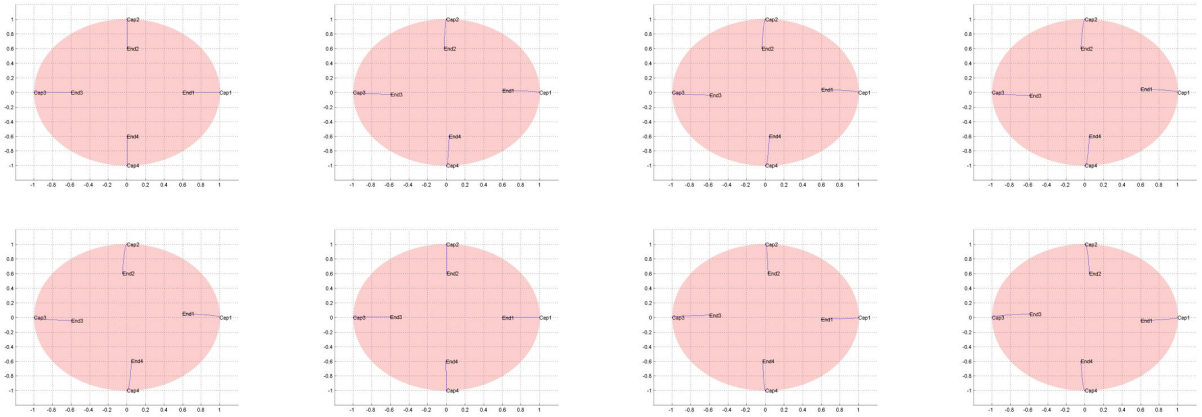

Fig. 11. Please zoom the .pdf for details. This picture is the analogous of Figure 10 but in this case the underlying kinematic model (22) assumes that the tendons only push.

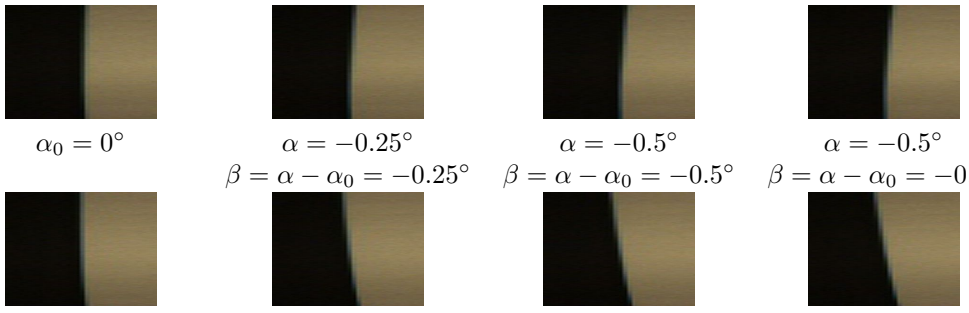

Fig. 12. Experimental results reproducing the experiments described in Section VI. The top right picture corresponds to one take with the eye in its initial configuration (zero cyclotorsion, $\alpha = 0°$). The pictures on its right have been obtained after one, two and three cyclic paths (34). The pictures on the second row have been obtained after one, two, three and four inverse cyclic paths (35).

in Section VI. Notice that on the real setup we can only control motors in position while simulations assume tendons controlled in velocity. For our purposes this, is not a real problem and the cyclic paths (30) and (32) can be easily translated into paths for the position of the motors. Specifically, let θ_1 be the position of the first motor and θ_2 be the position of the second motor. We considered the following cyclic path, which is intended to replicate what has been simulated in MATLAB:

$$\begin{array}{c} \boxed{\text{Initial configuration } \theta_1 = \theta_{1,0} \text{ and } \theta_2 = \theta_{2,0}} \\ \downarrow \\ \text{Move } \theta_1 \text{ to } \bar{\theta}: \quad \theta_{1,0} \xrightarrow{\theta_1} \bar{\theta} \\ \downarrow \\ \text{Move } \theta_2 \text{ to } \bar{\theta}: \quad \theta_{2,0} \xrightarrow{\theta_2} \bar{\theta} \\ \downarrow \\ \text{Move } \theta_1 \text{ to } \theta_{1,0}: \quad \bar{\theta} \xrightarrow{\theta_1} \theta_{1,0} \\ \downarrow \\ \text{Move } \theta_2 \text{ to } \theta_{2,0}: \quad \bar{\theta} \xrightarrow{\theta_2} \theta_{2,0} \\ \downarrow \\ \boxed{\text{Final configuration } \theta_1 = \theta_{1,0} \text{ and } \theta_2 = \theta_{2,0}} \end{array} \quad (34)$$

After each cyclic path, we took a picture of the panel in order to measure the cyclotorsion of the system. In order to measure the cyclotorsion angle, we used the same procedure described in Section II. The difference between the line orientation after and before the execution of the complete movement gives the cyclotorsion angle $\beta = \alpha_0 - \alpha$. The line orientation has been computed using the Hough transform [4]. The obtained results are shown in Figure 3. Qualitatively, results are similar to those obtained in simulation. The cyclotorsion initially increases and then reaches a maximum. In fact, after some cycles the cyclotorsion does not increase significantly. This is qualitatively in perfect agreement with the simulations which has been done with pull-only tendons model. As a second experiment, we consider the problem of reversing the previous path to see if it is possible to achieve an opposite the cyclotorsion as observed in the simulations. After having executed the path (34) three consecutive times, we have executed three times also the inverse path:

$$\begin{array}{c} \boxed{\text{Initial configuration } \theta_1 = \theta_{1,0} \text{ and } \theta_2 = \theta_{1,0}} \\ \downarrow \\ \text{Move } \theta_2 \text{ to } \bar{\theta}: \quad \theta_{2,0} \xrightarrow{\theta_2} \bar{\theta} \\ \downarrow \\ \text{Move } \theta_1 \text{ to } \bar{\theta}: \quad \theta_{1,0} \xrightarrow{\theta_1} \bar{\theta} \\ \downarrow \\ \text{Move } \theta_2 \text{ to } \theta_{2,0}: \quad \bar{\theta} \xrightarrow{\theta_2} \theta_{2,0} \\ \downarrow \\ \text{Move } \theta_1 \text{ to } \theta_{1,0}: \quad \bar{\theta} \xrightarrow{\theta_1} \theta_{1,0} \\ \downarrow \\ \boxed{\text{Final configuration } \theta_1 = \theta_{1,0} \text{ and } \theta_2 = \theta_{2,0}} \end{array} \quad (35)$$

The results of the experiment are shown in Figure 12. Remarkably, the obtained results are qualitatively in line with those obtained by simulating the kinematic model with push-only tendons. In particular, the cyclotorsion turns out to be reversible, in the sense that following the inverse path produces an opposite cyclotorsion. In Figure 12 it is shown that following the path (34) produces a negative cyclotorsion ($\beta < 0$) while following the inverse path (35) produces a positive cyclotorsion ($\beta > 0$). The maximum and minimum cyclotorsion that was experienced on the real setup are indicated in the following table[3]:

Minimum cyclotorsion	Maximum cyclotorsion	Range cyclotorsion
-0.75°	1°	1.75°

VIII. Conclusions and future works

We have presented a kinematic study of a tendon driven eyeball. The study was motivated by the necessity of understanding the cause of a cyclotorsion effect that was experienced on the real setup. The first part of the study was devoted to the development of a kinematic model of the tendon driven eye. The second part was focused on a qualitative comparison between data taken from the real setup and data obtained integrating the kinematic model. The comparison gave good results and leaves open the possibility of using the model for obtaining some quantitative data. Future works will investigate how useful the given model is for obtaining some quantitative data.

References

[1] D Biamino, G Cannata, M Maggiali, and A Piazza, *MAC-EYE: a tendon driven fully embedded robot eye*, 2005, pp. 62–67.

[2] F. Bullo and R. M. Murray, *Proportional derivative (PD) control on the Euclidean group*, vol. 2, June 1995, pp. 1091–1097.

[3] G Cannata and M Maggiali, *Implementation of Listing's Law for a Tendon Driven Robot Eye*, 2006, pp. 3940–3945.

[4] R. O. Duda and P. E. Hart, *Use of the hough transformation to detect lines and curves in pictures*, Comm. ACM **15** (1972), 11–15.

[5] R. M. Murray, Z. Li, and S. S. Sastry, *A mathematical introduction to robotic manipulation*, CRC Press, 1994.

[6] A D Polpitaya and B K Ghosh, *Modeling the dynamics of oculomotor system in three dimensions*, 2003.

[7] A D Polpitiya, B K Ghosh, C F Martin, and W P Dayawansa, *Mechanics of the eye movement: geometry of the listing space*, 2004.

[8] Ashoka D Polpitiya and Bijoy K Ghosh, *Modelling and control of eye-movement with musculotendon dynamics*, Proc of the 2002 American Control Conference ACC 2002, vol. 3, 2002, pp. 2313–2318.

[3] In simulation, the maximum and minimum cyclotorsion depend on the amplitude $\bar{\theta}$ of the cyclic path. The bigger is the amplitude the bigger is the observed cyclotorsion. This feature has been observed also on the real setup.